Electrochimica Acta 56 (2011) 2665–2675

Contents lists available at ScienceDirect

Electrochimica Acta

journal homepage: www.elsevier.com/locate/electacta

Hydrogen evolution under the influence of a magnetic field

Jakub Adam Koza[a,*], Sascha Mühlenhoff[b], Piotr Żabiński[c], Petr A. Nikrityuk[d], Kerstin Eckert[b], Margitta Uhlemann[a], Annett Gebert[a], Tom Weier[e], Ludwig Schultz[a], Stefan Odenbach[b]

[a] Leibniz Institute for Solid State and Materials Research IFW Dresden, P.O. Box 270116, D-01171 Dresden, Germany
[b] Dresden University of Technology, Institute for Fluid Mechanics, D-01069 Dresden, Germany
[c] AGH University of Science and Technology, Faculty of Non-Ferrous Metals, Department of Physical Chemistry and Metallurgy of Non-Ferrous Metals, 30 Mickiewicza Avenue, 30-059 Krakow, Poland
[d] CIC VIRTUHCON, Institute of Energy Processes and Chemical Engineering, Technische Universität Bergakademie Freiberg, Germany
[e] Forschungszentrum Dresden – Rossendorf, P.O. Box 51 01 19, 01314 Dresden, Germany

ARTICLE INFO

Article history:
Received 20 July 2010
Received in revised form 27 October 2010
Accepted 9 December 2010
Available online 22 December 2010

Keywords:
Lorentz force
Water electrolysis
MHD effect
micro-MHD
Desorption of hydrogen

ABSTRACT

The effect of a uniform magnetic field on the hydrogen evolution reaction (HER) during water electrolysis in 0.1 M Na_2SO_4 solution was investigated. Irrespective of the magnetic field orientation with respect to the electrode surface, the desorption of hydrogen is enhanced by the presence of the magnetic field. This effect is displayed by a reduction of the mean bubble size as well as a narrower bubble size distribution in a magnetic field. Moreover, it is shown that in the presence of an external magnetic field the fractional bubble coverage is strongly retarded. As a consequence the current density is increased since more active sites are available for the reduction processes. These effects are discussed with respect to the Lorentz force driven convection induced by a magnetic field. In order to resolve further the influence of a magnetic field applied in the perpendicular-to-electrode configuration, where the bulk Lorentz force is negligible, a numerical study has been performed. This revealed the mechanism of the improved desorption of a hydrogen bubble from the electrode surface. The numerical study has been validated by a model experiment. Most importantly, it is clearly demonstrated that a magnetic field superposed during water decomposition is a very effective method to intensify hydrogen evolution processes, and it should be possible to significantly improve the energetic efficiency of the hydrogen production via water electrolysis in a magnetic field.

1. Introduction

Hydrogen energy conversion technologies play an important role in the green energy development to overcome environmental problems. The electrolysis of water is an important technology for high purity hydrogen and oxygen gas production [1]. Considerable amount of attention has been given in order to understand the phenomena involved in the water electrolysis processes, especially the understanding of the convective effects, the mass transfer processes and the energy losses due to the IR-drop over the bubble layer at a gas evolving electrode has been greatly improved [2–7]. It has been shown that the surface area fraction covered by bubbles (θ) is a very important parameter which determines the upper operational current density and helps to estimate the ohmic voltage drop over the bubble layer [6,8]. Moreover, forced convection in the electrolyte has been shown to have a significant influence on the fractional bubble coverage, i.e. under forced convection the bubble coverage is greatly reduced [8–10]. This leads to a reduced ohmic voltage drop between electrodes and an improvement of the process efficiency [1].

Quite recently it has been shown that a superposed magnetic field during water electrolysis can significantly affect the process [11–14]. For instance the IR-drop between the working electrodes could be reduced by superposition of an external magnetic field [11,14]. A fractional bubble coverage and a reduced bubble size have been found affected by a magnetic field [12,14]. The origin of these effects is in Lorentz-force-driven convection, i.e. the so-called magnetohydrodynamic (MHD) effect, which introduces additional convection in the electrolyte [15]. It has also been shown that a localized convection can be induced close to a bubble due to a non-homogeneous current distribution in its vicinity [16,17], in analogy to the so-called micro-MHD effect [18].

The aim of this work is to investigate in detail the influence of a magnetic field on the hydrogen evolution reaction (HER) during water electrolysis by means of standard electrochemical techniques coupled with direct microscopic observations and numerical simulations.

* Corresponding author. Tel.: +49 351 4659 767; fax: +49 351 4659 541.
E-mail addresses: j.koza@ifw-dresden.de, kozaj@mst.edu (J.A. Koza).

0013-4686/$ – see front matter © 2010 Elsevier Ltd. All rights reserved.
doi:10.1016/j.electacta.2010.12.031

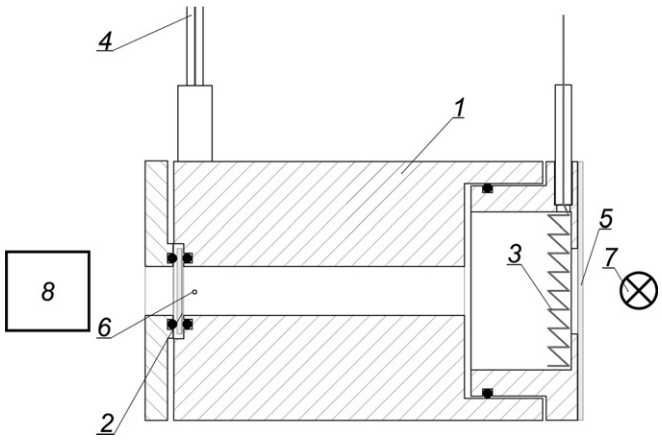

Fig. 1. Schematic representation of the experimental setup. *1* – cell, *2* – working electrode (glass/10 nm Ta), *3* – Pt-wire counter electrode, *4* – reference electrode, *5* – PMMA transparent window, *6* – Luggin capillary, *7* – cold light source, *8* – CCD camera coupled with optical microscope.

2. Experimental

The electrochemical experiments were carried out in two different cell types. The first one was a cylindrical Teflon cell schematically shown in Fig. 1, working in a three electrode configuration. The cell was designed to minimize edge effects [16]. As a working electrode 10 nm Ta have been sputtered onto a glass substrate with an active area of 1.33 cm^2 (*2* – Fig. 1). At this thickness, the Ta layer is transparent which allows the in situ observation of gas bubbles evolving at the electrode surface. As a counter electrode, a Pt wire (*3* – Fig. 1) was used and as a reference a $Hg/Hg_2SO_4/K_2SO_{4(sat.)}$ electrode (MSE, +640 mV vs. SHE) was employed (*4* – Fig. 1). The working electrode potential was controlled by a Jaissle potentiostat (PGU 10 V to 100 mA). The cell was designed in a way that the both sides, cathodic and anodic, were transparent and placed in a light path. The working electrode surface was monitored from the back by a CCD camera (Baumer TXD13) coupled with an optical microscope (Navitar, *8* – Fig. 1). A cold light (*7* – Fig. 1) was used as a light source. The experiments were carried out from a 0.1 M Na_2SO_4 aqueous solution, adjusted to pH = 3 by means of sulphuric acid. A magnetic field has been superposed during the experiments in two configurations relative to the electrode surface, i.e. in the perpendicular to a horizontal electrode (Fig. 2a) and in the parallel to a vertical electrode configuration (Fig. 2b). In the case of the perpendicular-to-electrode configuration the magnetic field was generated by a resistive tube magnet which produces a flux density of 70 mT uniformly distributed across the electrode surface. In the parallel configuration, a homogeneous magnetic field was applied by a water cooled electromagnet (HV7, Walker Scientific) with flux densities up to 750 mT.

To resolve the micro-convective flow around the bubbles, model experiments coupled to numerical simulations (Section 2.1) were performed. To guarantee a high resolution of the flow field under

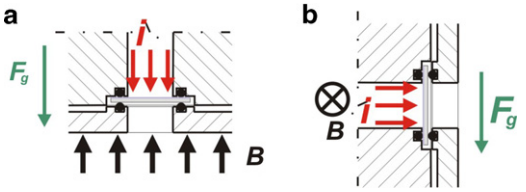

Fig. 2. Relative to the electrode surface magnetic field orientations: (a) perpendicular-to-electrode (⊥) and (b) parallel-to-electrode (||) configuration. F_g stands for the gravitational force.

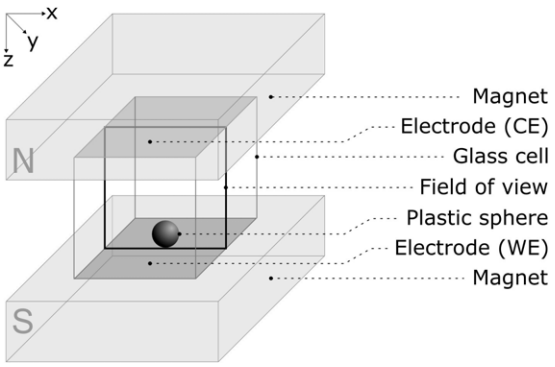

Fig. 3. Schematic representation of the experimental setup used for the model experiment using a non-conducting plastic sphere as an artificial bubble between two horizontal electrodes and under the superposition of a vertical homogeneous magnetic field.

steady-state conditions we substitute the small and detaching bubbles by a larger non-conductive plastic sphere (diameter 3.2 mm). To study the flow field by particle image velocity (PIV) technique, a second cell type consisting of a cuboid glass cell ($10 \times 10 \times 10\ mm^3$) was used (Fig. 3). A horizontal Cu plate at the bottom of the cell was utilized as working electrode onto which the sphere was fixed in its centre. Another Cu plate at the top served as a counter electrode. The experiments were carried out in a two electrode configuration in the galvanostatic mode. Currents of 5–15 mA have been applied. The electrolyte was a 0.5 M $CuSO_4$ solution adjusted to pH = 3 by means of H_2SO_4. The Cu deposition system has been chosen in order to guarantee that no gas evolution takes place. A magnetic field of 800 mT was superposed parallel to the electric field by a set of two large NdFeB magnets ($40 \times 40 \times 20\ mm^3$) in an arrangement that gives a very homogenous magnetic field over the whole volume of the cell, which was placed in the middle of magnets gap. To visualize the convection polystyrene particles with a size of $9.6 \pm 0.1\ \mu m$ and a density of 1.005 g cm^{-3} were added to the solution. A laser-light-sheet was irradiated from the side at the middle position of the plastic sphere to illuminate a two dimensional section of the cell volume in the x-z-plane. The reflections of the particles were recorded perpendicularly via a 21-2M30 DALSA-camera operating in 2×2 binning mode (800×600 px) and a macro optic. To evaluate the velocity a commercial software PIVView [19] using the cross-correlation algorithm with a 50% overlap of the 48×48 px interrogation windows was employed.

All experiments were carried out at room temperature.

2.1. Numerical simulation

To model the interplay between the shape of the bubble, electric current density and the fluid flow we use a computational domain in the form of a cylinder. The bubble of radius R_0 is placed near the bottom of the cylinder in such a way that its symmetry axis concurs with the axis of the domain. Thus, a cylindrical coordinate system (r, θ, z) can be used to model the fluid flow and electrical current distribution around the sphere. The entire cylindrical domain extends over $H/R_0 = 7$ and $R/R_0 = 6$ in axial and radial directions, respectively. It is bounded at the top and bottom by electrodes of different potentials, where the bubble is located in the centre of the lower one. In order to distinguish between the liquid and the gas phases we introduce a volume of fluid variable ε which has the value of unity and zero for all finite volume cells occupied by the liquid and the gas, respectively. This variable is calculated only once by initialisation of the bubble location.

Before we proceed with the formulation of the mathematical model let us describe shortly the main physics of the process we

want to model. The simulations are focused on the perpendicular-to-electrode configuration, i.e. the magnetic field is parallel to the electric current far away from the electrode surface. Hence, no Lorentz force exists in the absence of a bubble. The electric conductivity, σ_B, of the bubble was set to zero. Consequently, a bending of the current lines occurs around the bubble. Hence, the current density is not longer parallel to B, and a Lorentz force, $\vec{F}_L = \vec{j} \times \vec{B}$, appears. This force drives a swirling flow around the bubble which is governed by the incompressible Navier–Stokes (N–S) equation given in the steady state as:

$$\nabla \cdot \vec{V} = 0 \tag{1}$$

$$\rho(\vec{V} \cdot \nabla)\vec{V} = -\nabla p + \mu \Delta \vec{V} - \frac{\mu}{K}\vec{V} + \vec{F}_L \tag{2}$$

where $\vec{V}$ refers to the velocity vector with the components (V_r, V_θ, V_z) and p to the pressure; ρ, μ and K are the density, the dynamic viscosity and a penalty function explained later, respectively. Note that F_L has an azimuthal component, only, in particular $F_{L\theta} = -\sigma B_z(\partial\varphi/\partial r)$. Therefore, the symmetry of the problem justifies an axisymmetric formulation, i.e. all derivatives in azimuthal direction in Eq. (2) are neglected. The electric current, necessary to calculate F_L, follows from the simplified Ohm's law, $\vec{j} = \sigma\nabla\varphi$, where the term $\sigma(\vec{V} \times \vec{B})$ is neglected due to a small magnitude of the microscale velocity in numerical simulations. The electric potential φ can be computed by applying the charge conservation, $\nabla \cdot \vec{j} = 0$, via:

$$\frac{1}{r}\frac{\partial}{\partial r}\left(r\sigma\frac{\partial\varphi}{\partial r}\right) + \frac{\partial}{\partial z}\left(\sigma\frac{\partial\varphi}{\partial z}\right) = 0 \tag{3}$$

where the electrical conductivity (σ) is calculated as follows:

$$\sigma = \begin{cases} \sigma_l = \text{const.}, \text{if} \quad \varepsilon = 1(\text{liquid}) \\ \sigma_B = 0, \text{if} \quad \varepsilon = 0(\text{gas}) \end{cases} \tag{4}$$

The boundary conditions for the electric potential are Dirichlet conditions on top and bottom, i.e. $\varphi = \varphi_T$ and $\varphi = \varphi_B$, calculated from the given E_z near the surface as follows $\varphi_T = E_z H$, $\varphi_B = 0$. On the axis and the side boundaries of the computational domain Neumann conditions, $\partial\varphi/\partial r = 0$ were applied. For the velocity, the no-slip condition holds at all solid walls. To force no-slip at the bubble surface, we use the following penalty variable:

$$K = \begin{cases} \infty & \text{if} \quad \varepsilon = 1 \\ 0 & \text{if} \quad \varepsilon = 0 \end{cases} \tag{5}$$

In order to speed up the convergence we adopted Patankar's [25] linearization of the source term $S = \mu/K \cdot \vec{V}$ in Eq. (2), given by:

$$S = S_C + S_P\phi_P \quad \text{with,} \quad S_C^v = 0, \quad S_P^v = -\mu\frac{1}{K} \tag{6}$$

where ϕ_P refers to the value of principal variable (V_r or V_θ). Since only the flow field driven by the Lorentz force is of interest, buoyancy and interfacial tension forces acting at the contact line are neglected.

The bottom of the domain was treated as no-slip and the top and the side walls were assumed to be stress free.

The N–S equations and the electric potential equation given by Eqs. (1)–(3) have been discretized by a finite-volume, finite-difference based method. The SIMPLE algorithm with a collocated-variables arrangement was used to calculate the pressure and the velocities [20]. The Rhie and Chow [21] stabilization scheme was used for the stabilization of the pressure–velocity coupling. The convective terms were discretized by a central difference second order scheme with deferred correction [20]. The system of linear equations was solved by Stone's strongly implicit procedure (SIP). For details of the numerical schemes and the matrix solver used we refer to [20].

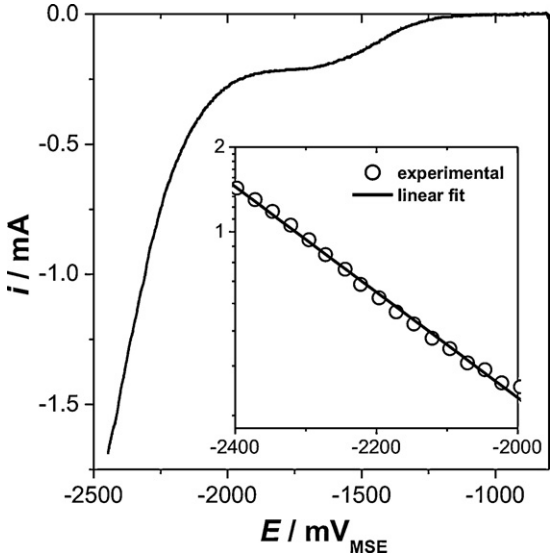

Fig. 4. LSV obtained for Na_2SO_4 electrolyte at Ta electrode without magnetic field (20 mV s^{-1}). The inset shows the water decomposition region in Tafel coordinates.

For the flow simulation the following values were used: $B_z = 1$ T, $E_z = -\nabla \cdot \varphi = 100$ V m^{-1}. The density and the dynamic viscosity were set to $\rho = 1000$ kg m^{-3} and $\mu = 1.4 \cdot 10^{-3}$ m^2 s^{-1}, respectively. The electrical conductivity of the liquid phase was set to $\sigma = 1.35$ A/V m. The grid used in the simulations has 250×300 control volumes in the radial and axial directions, respectively.

3. Results and discussion

3.1. Hydrogen evolution under the influence of a magnetic field – in situ investigation

In Fig. 4 the linear sweep voltammogram (LSV) obtained for 0.1 M Na_2SO_4 electrolyte at the Ta electrode without a magnetic field is shown. Two distinctive regimes can be seen from the LSV. From a potential of about -1200 mV_{MSE} to about -1800 mV_{MSE} a proton reduction peak is observed followed by a sharp increase of the current density related to the water decomposition reaction. Based on the shape of the LSV the potential for the potentiostatic experiments have been chosen. In order to prevent any influence

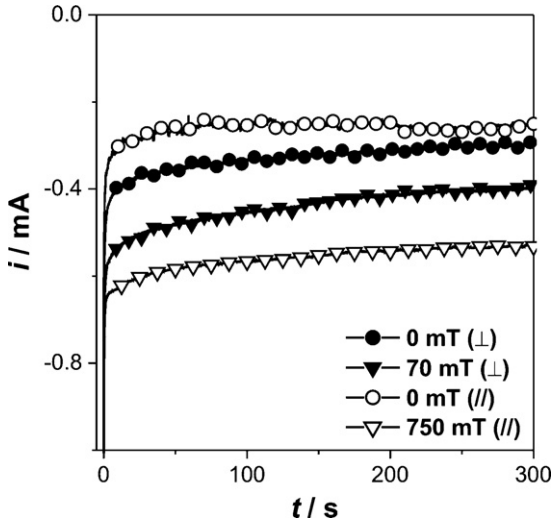

Fig. 5. Current–time transients obtained without and with a magnetic field applied in both relative to the electrode surface configurations.

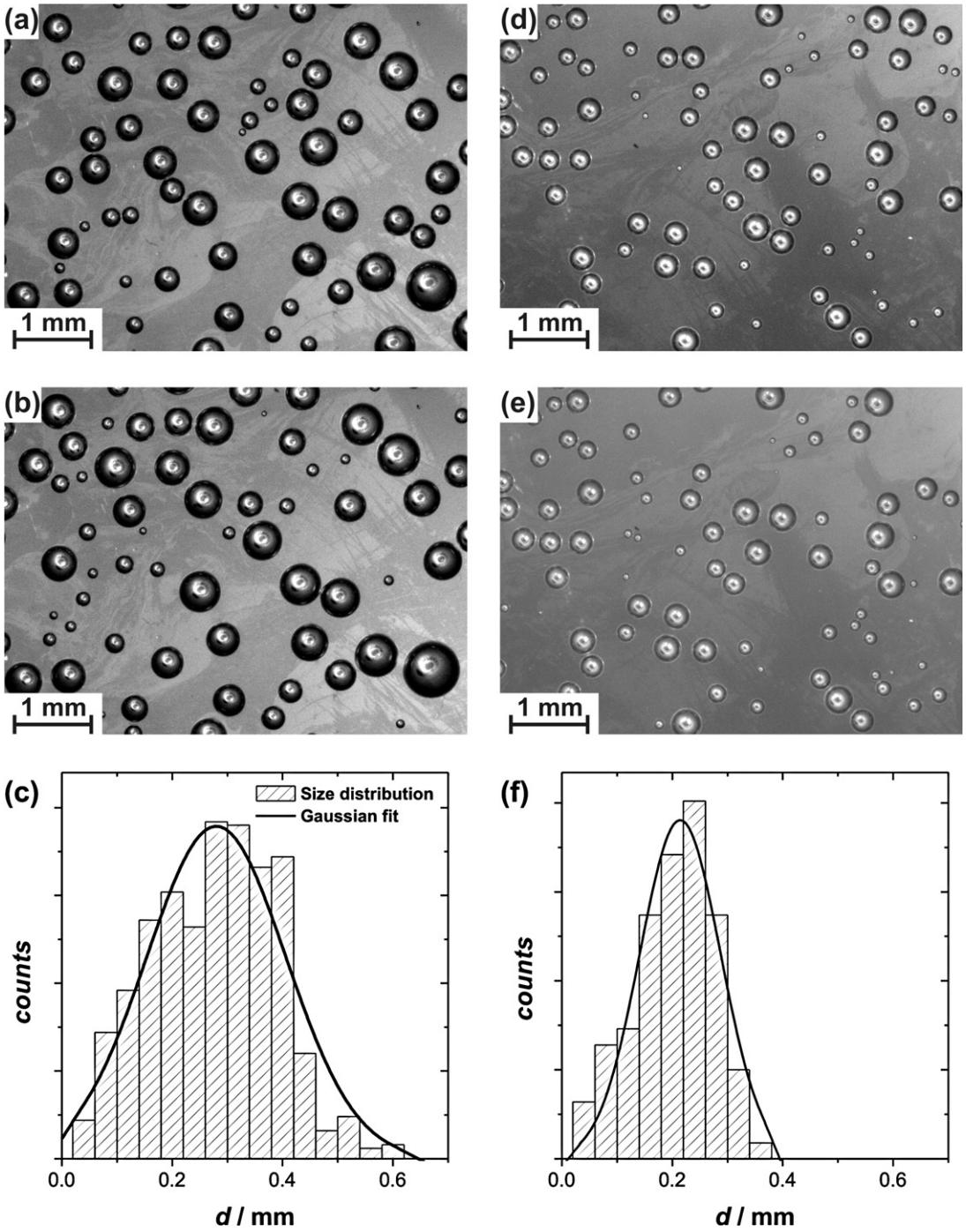

Fig. 6. Hydrogen bubbles formed at the electrode surface in the stationary regime observed without a magnetic field (a and b) and in the perpendicular to the electrode magnetic field (B = 70 mT) (d and e). Images (b and e) were taken at about 60 s longer reduction time than (a and d) and represent a time sequence. The distribution of the bubble size obtained without a field (c) and in the perpendicular to the electrode magnetic field (B = 70 mT) (f).

of the bulk MHD stirring on the mass transport of H^+ ions towards the electrode it was decided to work in the water decomposition potential range which is in charge transfer control (inset of Fig. 4). On the other hand, if the applied potential is too high, a very intensive bubbling would be present which can be of higher magnitude than the magnetic field influence. Because of the above reasons a potential of $-2100\,mV_{MSE}$ has been chosen for the potentiostatic experiments.

In Fig. 5 the current–time transients obtained for the HER at the Ta electrodes without and with a magnetic field superposed in both relative-to-electrode configurations are shown. It is apparent that the stationary current density is increased in a field irrespective of its relative to the electrode orientation. Considering the charge transfer control of the HER, the observed current enhancement has to be of a different origin than the mass transport of the reactants. It is well established that the current is proportional to the active surface area irrespective of the reaction rate limiting step [22]. This strongly suggests that the current enhancement is caused by a reduced coverage of the electrode surface by the hydrogen bubbles. In order to investigate this further, an in situ microscopic investigation of the electrode surface during hydrogen evolution has been performed.

In Fig. 6 images of the electrode surface taken during the evolution of hydrogen under stationary conditions without (a and b) and with a magnetic field (70 mT) superposed in the perpendicular-to-electrode configuration (d and e) are shown. It is apparent that the bubble size is reduced in the field what is clearly shown by the bubble size distribution depicted in Fig. 6c and f. Additionally, the distribution of the bubble size is narrower in the field. The maximum diameter in the Gaussian curve (Fig. 6c and f) represents the break-off diameter. Without magnetic field and a current density of 2.2 A m^{-2} the bubble release diameter is of about 0.6 mm and decreases in 70 mT magnetic flux density to about 0.4 mm at a current density of 3 A m^{-2}. This is in agreement with results of Vogt et al. [6,8]. They found that at low current densities the break-off diameter is significantly affected. Moreover, they exhibit that all data converge to a bubble release diameter of 0.7 mm without current and decreases to a value of about 0.5 mm at 4 A m^{-2} in a horizontal electrode setup.

In a horizontal electrode geometry it is possible to estimate the bubble diameter at the moment of detachment, as proposed by Eigeldinger and Vogt [8]. They used a force balance between the buoyancy and the interfacial tension to calculate the break-off diameter. For the horizontal electrode arrangement and stagnant electrolyte, using Eqs. (17) and (21) of Eigeldinger and Vogt [8], assuming equality of advancing and receding contact angle, the break-off radius can be estimated on a basis of Eq. (7).

$$R = \sqrt{\frac{\gamma}{k \cdot g \cdot (\rho_L - \rho_G)}} \tag{7}$$

where γ is the interfacial tension (70 mN m^{-1} g^{-1}); g is the gravitational acceleration (10 m s^{-2}); $\rho_L - \rho_G$ is the density contrast between the bubble and the electrolyte (10^3 kg m^{-3}); k is the geometry factor (0.5), nearly the same for all contact angles.

With Eq. (7) we arrive at the bubble break-off diameter of 1.7 mm which is about 3–5 times larger as that which was observed (Fig. 6a–c), yet, of the same order of magnitude. However, bubble removal occurs frequently after coalescence, as exemplary shown in Fig. 7, hence in a situation which is not correctly reflected by this simple force balance equation. This coalescence of bubbles leads to a change in the pressure field and additional convection is induced. Moreover, a detached bubble formed after coalescence draws away the electrolyte below, leading to a lower pressure in this region. As a consequence a small bubble in the vicinity (Fig. 7c) is also removed from the electrode surface. Due to these phenomena the observed bubble break-off diameter is considerably lower then the calculated by Eq. (7). The lower bubble size in an applied magnetic field is due to the induced magneto-convection as discussed later.

In Fig. 8 images of the electrode surface during bubble evolution without (a and b) and in the parallel to the electrode magnetic field (d and e) together with their size distribution (c and f) are shown. The results obtained in the parallel magnetic field are qualitatively the same as in the perpendicular configuration, i.e. reduced bubble size and narrower size distribution in a magnetic field is achieved. However, the bubble size obtained without a field is reduced in the vertical electrode configuration (Fig. 8a–c) in comparison to the horizontal electrode case (Fig. 6a–c). The reason of this is a different electrode orientation in these cases. The bubble can be detached from the electrode when the difference of the gravitational force and buoyancy force exceeds the adhesion force [8]. The evolution of bubbles at a vertical electrode introduces a strong convection near the electrode surface pointing upwards due to the buoyancy force acting on the bubbles. As a consequence of additional electrolyte stirring near the boundary layer, the size of the bubbles is reduced. Moreover, in the vertical electrode configuration, detached bubbles from the lower part of the electrode (Fig. 9d indicated by an arrow) moving along the electrode can collect all the bubbles on

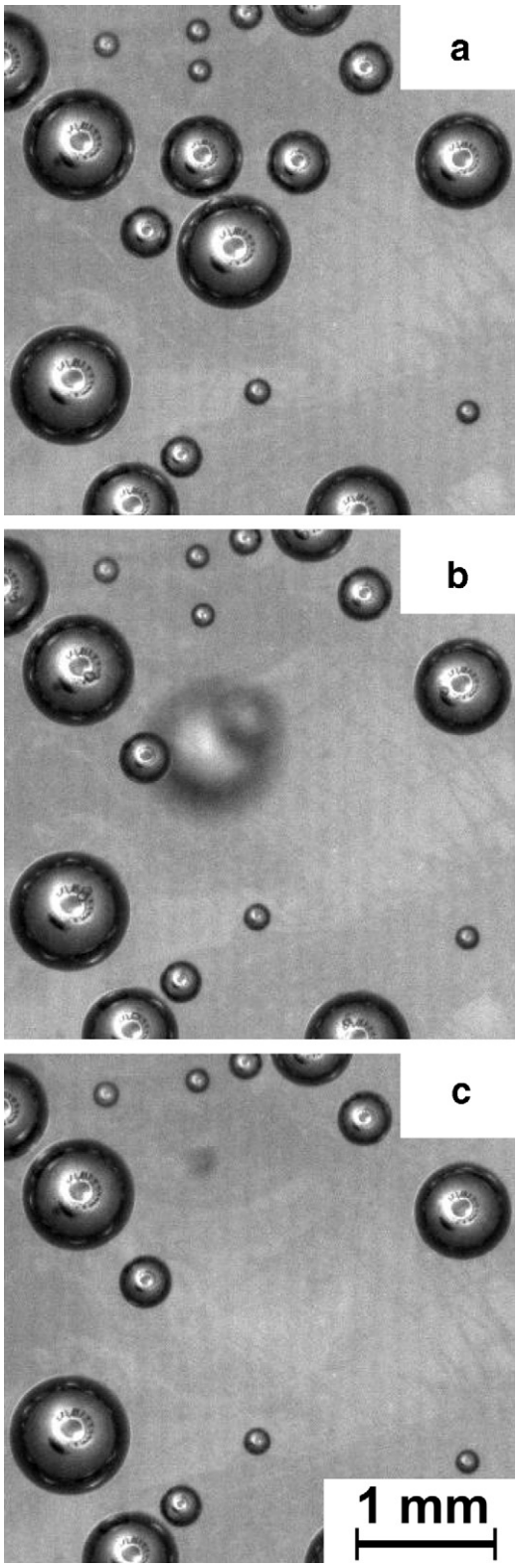

Fig. 7. A time sequence showing coalescence of two bubbles phenomenon and the micro-convection effect induced by a desorbed bubble. Stationary conditions, 0 T, perpendicular-to-electrode configuration, images (b and c) were taken 0.24 and 0.48 s, respectively, after image (a).

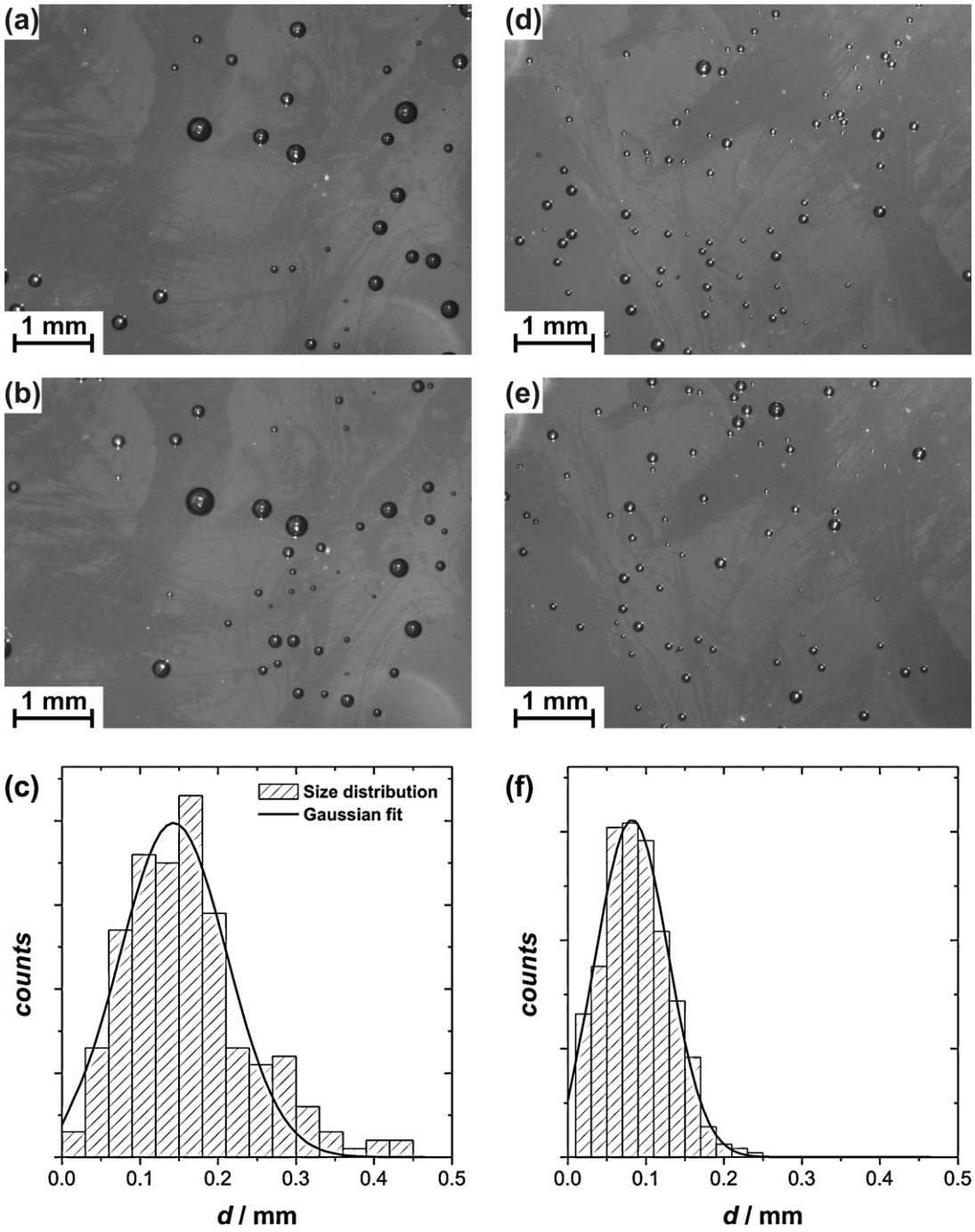

Fig. 8. Hydrogen bubbles formed at the electrode surface in the stationary regime observed without a magnetic field (a and b) and in the parallel to the electrode magnetic field (B = 750 mT) (d and e). Images (b and e) were taken at about 60 s longer reduction time than (a and d) and represent a time sequence. The distribution of the bubble size obtained without a field (c) and in the parallel to the electrode magnetic field (B = 750 mT) (f).

their way upwards. This can easily be seen in Fig. 9d–g. However, this effect is not always observed due to the two-phase convection phenomena at the vertical gas-evolving electrode [4], what can be seen in Fig. 9a–c. The bubble detached at the bottom of the electrode (Fig. 9a – indicated by an arrow) does not coalesce with other bubbles located in its trajectory. The size of the detached bubble, the distance to the nearest neighbour as well as its size are the factors determining whether the bubble coalesces with others or not. The shorter the distance and the larger the size of the nearest bubble the higher is the coalescence probability. This leads to a reduced bubble size in the vertical electrode configuration in comparison to the horizontal electrode arrangement observed without a magnetic field. Moreover, the bubble coverage fraction, as will be quantitatively shown later on, is reduced in the vertical electrode configuration when compared to the horizontal arrangement. This is in agreement with previously reported results [8,10], where in a stagnant electrolyte a reduced coverage fraction of hydrogen bubbles has been noticed in the vertical electrode arrangement in comparison to the horizontal case.

The mean bubble size and the size distribution has been calculated for different magnetic flux densities for both magnetic field to the electrode configurations and summarized in Fig. 10. In Fig. 10 full weight at half maximum (*FWHM*) of the Gaussian fit represents the bubble size distribution.

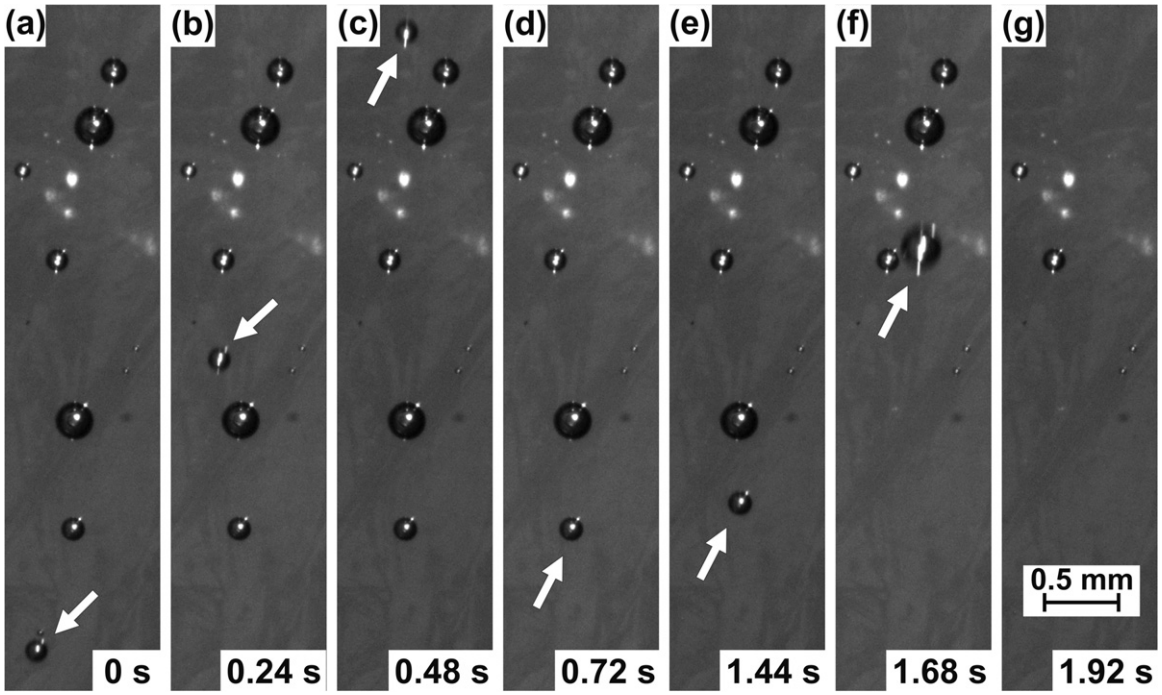

Fig. 9. Set of optical images representing a time sequence, which shows the two-phase convection profile and the coalescence of bubbles process at vertical electrode. Image (a) was taken after about 5 min of the electrolysis but as initial conditions is referred as 0 s. B = 250 mT, parallel-to-electrode configuration.

From Fig. 10 it is apparent that the bubble mean size as well as bubble size distribution is reduced in a magnetic field irrespective of the relative to the electrode surface orientation. Similar results have also been observed by Matsushima et al. [12] for oxygen evolution at a transparent fluorine-doped tin oxide (FTO) coated glass electrode in a parallel-to-electrode magnetic field, i.e. a reduced bubble size was reported. As mentioned the stationary current density is enhanced in a magnetic field regardless of its configuration. It was suggested that the reason for this is a reduced fraction of the electrode surface covered by bubbles. To investigate this in detail the coverage fraction (θ), defined as an area obtained by projection of the bubble to the electrode surface normalized to the overall electrode area [23], has been calculated at different magnetic flux densities on the basis of the microscopic investigations (Figs. 6 and 8). The influence of a magnetic field on the electrode area fraction covered by the bubbles with respect to the magnetic flux density and relative to the electrode surface magnetic field orientation is shown in Fig. 11.

It is obvious that the coverage is strongly reduced in a field for both magnetic field configurations. These results are in agreement with previously published results by Matsushima et al. [12]. However, the perpendicular magnetic field is more effective and the coverage is reduced by 50% at flux density of 70 mT, whereas in the parallel field 750 mT is necessary to achieve the same effect. This supports the hypothesis that the current is increased due to the increased active surface area in a field. However, the current enhancement observed in the field is far greater than the reduction of the surface coverage fraction, especially in the vertical electrode arrangement, where the coverage is quite low even without a magnetic field (about 4% – Fig. 11b). At this point it seems more correct to assign the current to the electrode as an integral value of discrete currents to active sites available for hydrogen reduction and bubble nucleation, which are limited, rather than to the whole electrode area. The flux density of 70 mT and 750 mT for perpendicular- and for parallel-to-electrode magnetic field, respectively, results in reduction of the coverage of about 50%. This leads to a rough estimate of twice as high stationary current density reached in a field as compared to the non-magnetic field cases. This in turn fits relatively well to the current enhancement obtained in this study (Fig. 5). It was observed, by analysis of a large set of images, that bubbles are formed at specific sites repetitively rather then randomly over the whole electrode surface. This strongly supports the explanation based on preferred active sites for hydrogen bubbles formation. However, it has to be stressed that the bubble evolution processes are dynamic and more importantly, the resolution of the microscope is limited, i.e. small bubbles (below few μm) as well as small defects, which may serve as active sites, are not visible, and thus the above discussion should be considered as a rough estimation.

Nevertheless, it is obvious that a magnetic field superposed during hydrogen evolution significantly affects the process, i.e. it leads to a reduced bubble size, narrower size distribution and a reduced surface coverage, irrespective of the magnetic field to the electrode surface configuration. The reason for this is the Lorentz-force-driven convection which induces additional stirring, i.e. MHD effects. This will be further discussed in the next sections.

3.2. Model experiments and numerical simulation

The results of the numerical simulation are compiled in Fig. 12. Due to the symmetry of the problem, it is sufficient to display only one half of the bubble. Fig. 12a provides the vector plot of the electric current distribution. The curvature of the current lines in the vicinity of the bubble is clearly visible resulting from its vanishing electrical conductivity. Hence, the electric current receives a radial component directed away from the bubble in the upper half and towards the bubble in the lower half. Consequently, an azimuthally directed Lorentz force, $F_{L\theta} = j_r B_z$, appears, pointing out of the plane of the paper in the upper half of the bubble, and into the plane of the paper in the lower half of the bubble. This is visualized in the Lorentz force distribution plot shown in Fig. 12b. As a result, a primary swirling flow in the azimuthal direction occurs, which circulates in clockwise direction around the upper half of the bubble, when looking from above. In contrast, the flow around the lower

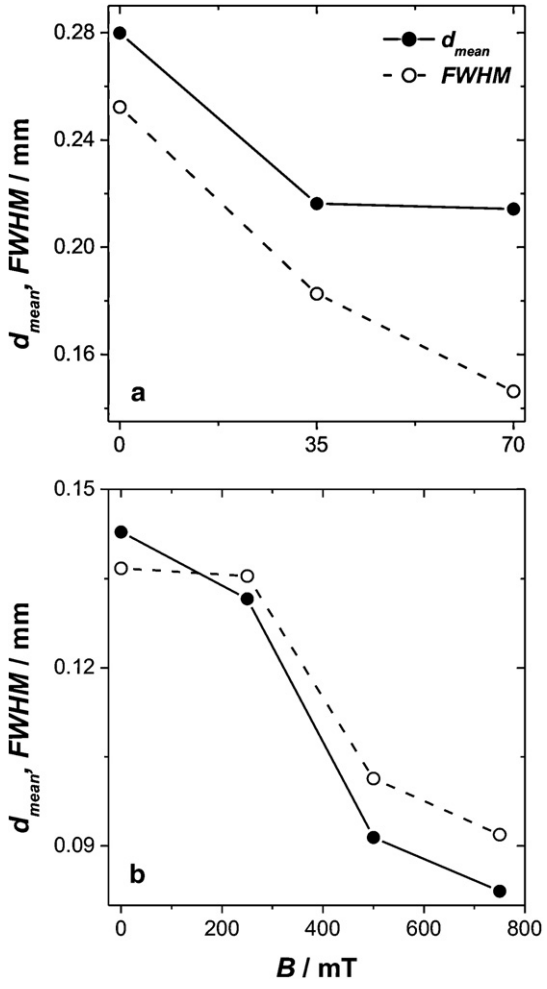

Fig. 10. Mean bubble size and size distribution (*FWHM*), calculated by the Gaussian fit (Figs. 7c and f and 8c and f), vs. magnetic flux density dependencies obtained in perpendicular to the horizontal (a) and parallel to the vertical electrode (b) configuration.

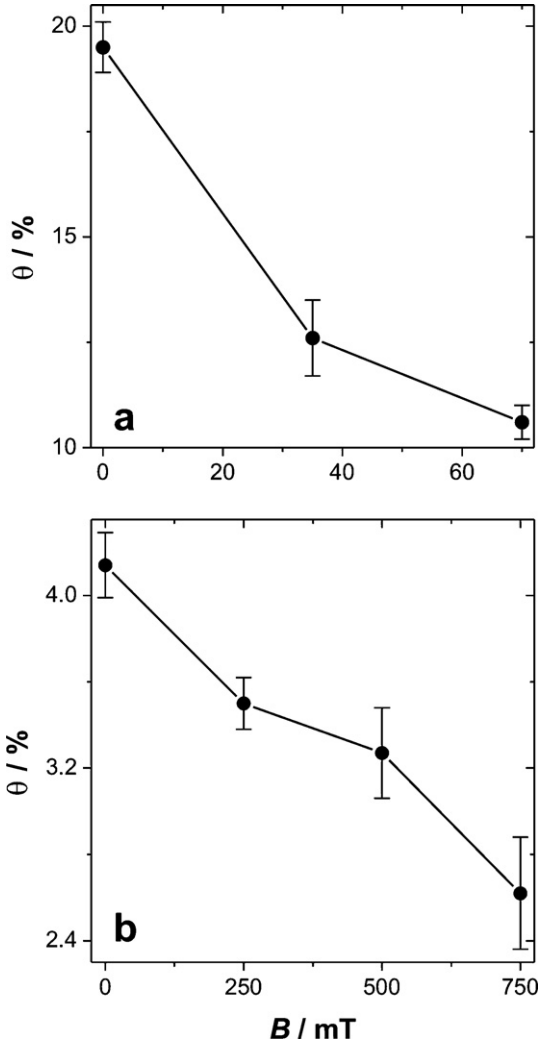

Fig. 11. Surface coverage of hydrogen gas bubbles on the electrode vs. magnetic flux density obtained in perpendicular to the horizontal (a) and parallel to the vertical electrode (b) configuration.

half of the bubble rotates in counter-clockwise direction. This is depicted in the contour plot of the azimuthal velocity distribution shown in Fig. 12c. However, the velocity of the swirling flow around the upper half of the bubble is considerably larger. This is a direct consequence of the asymmetry in the bending of the electric current lines. The resulting radial current components are larger in the upper half, hence the Lorentz force, too, as compared to the lower half.

As soon as fluid elements start to rotate with a velocity V_θ, they experience a centrifugal acceleration V_θ^2/r. Hence, they acquire an outward radial velocity component. Due to mass conservation, this fluid has to be replaced by fluid drawn axially towards the bubble. As a result, a secondary flow is established consisting of two torii which appear as a double vortex in the two-dimensional section (Fig. 12d).

This secondary flow is exactly reproduced by the PIV measurements in the experiment (Fig. 13). The non-conducting plastic sphere, serving as a model of the bubble, sits in the centre of the bottom electrode. Fig. 13 is terminated on the top by the upper electrode. The cuboid glass cell is intersected by the laser light sheet in the *x*–*z*-plane. The light sheet, coming from the right-hand side, hits the centre of the sphere (see the bright rim at its perimeter). The light scattered by the particles within this light sheet is used to calculate the velocity field via a standard cross-correlation algorithm. The velocity field is shown as a vector plot in the *x*–*z*-plane with a superposed contour of the sphere (Fig. 13). The opaqueness of the sphere excludes an access into the region directly behind the sphere. However, due to the (quasi-) symmetry of the problem all necessary information is already contained in the right half of Fig. 13. As already discussed above, the secondary flow pattern is characterized by an axial flow towards the sphere with a characteristic velocity of 2 mm s^{-1}. The flow turns radially outwards on the height of the upper half of the sphere. Due to mass continuity, a pair of counter-rotating vortices appears. The lower vortex, situated in the lower right corner of the light sheet of Fig. 13 rotates clockwise and has approximately the same size as the sphere. The maximum velocity is about 0.4 mm s^{-1}. The second vortex of comparable extension in the right upper half rotates in counter-clockwise manner. The flow direction in both vortices is independent of the direction of the electric field. It remains unchanged upon a current reversal from −7 mA to +7 mA.

The presented situation bears a strong analogy to the rotating disc electrode. The disc rotation is mimicked by the Lorentz force. The resulting complex flow structure has a marked impact onto the pressure distribution around the bubble which is shown in Fig. 12e: a low-pressure region forms above the bubble. This imbalance of pressure around the bubble creates an additional lift force which significantly facilitates the bubble detachment.

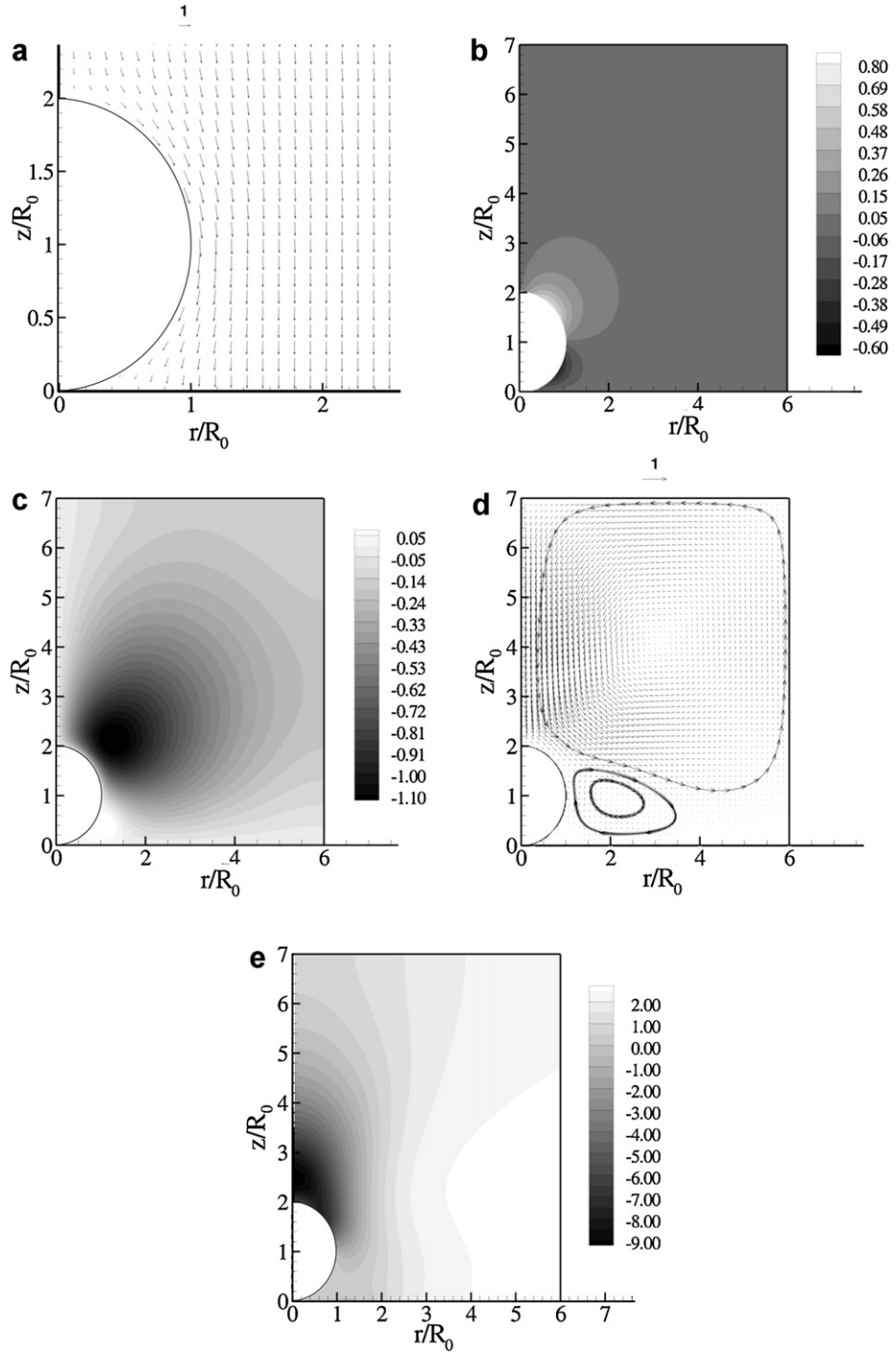

Fig. 12. Results of numerical simulation of a bubble in a uniform perpendicular-to-electrode magnetic field: (a) zoomed nondimensional electrical current $\vec{j}/E_z\sigma$ distribution, (b) distribution of nondimensional azimuthal component of the Lorentz force $F_L/E_z\sigma B_z$, (c) nondimensional azimuthal w/w_0 velocity distribution, (d) nondimensional meridional $\vec{u}/u_0$ velocity distribution, and (e) nondimensional pressure $p/10^{-8}$ distribution obtained at $B = 1$ T, $w_0 = 10^{-5}$ m s^{-1}, $u_0 = 10^{-9}$ m s^{-1}, $2R_0 = 10^{-4}$ m.

4. Discussion

As shown in previous sections a superposed magnetic field during the gaseous hydrogen evolution significantly affects the process, irrespective of its relative-to-electrode configuration. This is manifested by a reduced electrode fraction covered by bubbles, reduced bubble size and narrower size distribution. The effect can be divided into two categories. At first we will consider the parallel-to-electrode configuration. In order to simplify the discussion and omit the coalescence phenomena [4], the horizontal electrode will be considered. In the parallel to the electrode surface magnetic field, the electric and magnetic fields are perpendicular to each other resulting in a macroscopic convection due to the Lorentz force acting in the bulk, i.e. a classical MHD effect [15]. A bubble at the electrode surface acts as an obstacle in the flow and a hydrodynamic drag acting on the bubble will be induced [8,11,24]. This leads to a reduced bubble size and its faster desorption from the electrode surface, and as a consequence depolarisation of the electrode is noticed [11,14]. Moreover, the coalescence of the bubbles is enhanced [14], which leads to an improved desorption of bub-

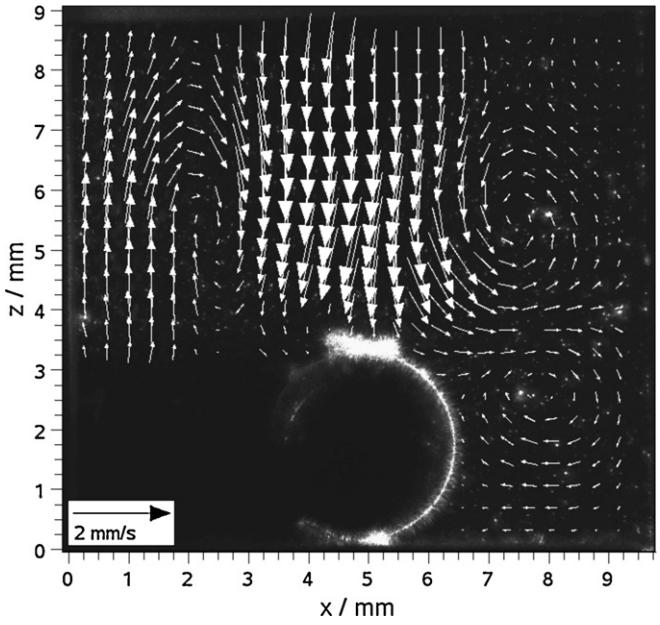

Fig. 13. Velocity distribution around a non-conducting plastic sphere as an artificial bubble between two horizontal electrodes and under the superposition of a vertical homogeneous magnetic field.

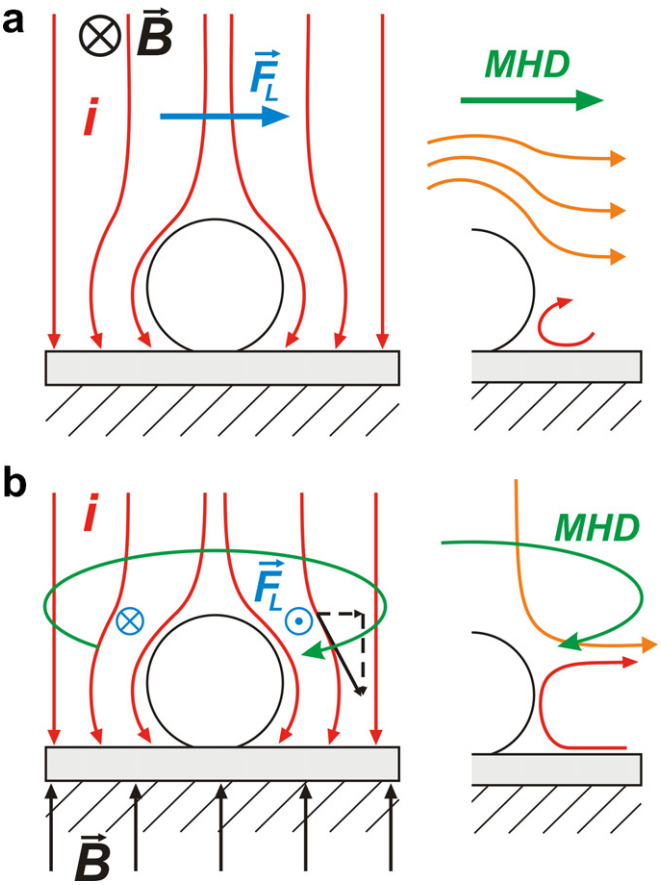

Fig. 14. Schematic representation of the current distribution together with direction of Lorentz force (left hand side) and characteristic convection patterns (right hand side) in the vicinity of a bubble obtained in the parallel- (a) and perpendicular-to-electrode (b) magnetic field configuration.

bles from the electrode surface. A schematic representation of these phenomena is shown in Fig. 14a. This effect is qualitatively the same as obtained under forced convection [8,9]. They have also shown a dramatic reduction of the electrode fraction covered by the bubbles and an improved coalescence of bubbles under forced convection condition.

In contrary, in the perpendicular magnetic field, where the electric field and magnetic field, in bulk, are aligned parallel, the Lorentz force is expected to be minimized. However, the mean bubble size and its distribution (Fig. 10a) as well as the bubble coverage fraction (Fig. 11a) are reduced in a field. The reason for this is seen in a Lorentz-force-driven convection which arises due to a non-homogenous current distribution in the vicinity of the bubble (Fig. 14b – left hand side and Fig. 13a and b). As a result a secondary flow is induced, which facilitates the removal of the bubble from the electrode surface (Fig. 12b – right hand side and Fig. 13c), i.e. the desorption of a hydrogen bubble from the electrode surface is enhanced in a magnetic field. A similar influence of a perpendicular magnetic field on the HER accompanying the metal deposition has already been reported [17]. Additionally it has to be mentioned that magnetic field induced convections are very complex already at flat electrodes without gas evolution especially in small cell geometries as shown by Cierpka et al. [26].

However, the situation presented by the numerical simulation and the model experiment is simplified to a single bubble. At a real electrode many bubbles are present during gas evolution which may lead to complex interactions between them as already shown in Fig. 7, where the coalescence of two bubbles is visible (a and b). After coalescence, the large bubble is immediately removed from the electrode surface (Fig. 7b). This, in turn, induces microconvective phenomena below the desorbed bubble [5], the pressure field is affected and the bubble in the vicinity is sucked away from the electrode surface. First attempts have been made to visualize the influence of a magnetic field when more bubbles at the electrode are present. However, the flow pattern is very complex and further systematic investigations supported by numerical simulations are necessary in order to resolve it.

5. Conclusions

It has been clearly demonstrated that the superposition of a magnetic field during water electrolysis, regardless of its orientation relative to the electrode surface, significantly affects the process. Improved desorption of hydrogen bubbles from the electrode surface, reduced fractional bubble coverage and mean bubble size as well as narrower bubble size distribution in the presence of a magnetic field have been found. The improved desorption of hydrogen bubbles from the electrode surface and a reduced coverage fraction in a magnetic field is advantageous for water electrolysis technology as the efficiency of the process is greatly improved, even at low magnetic flux density. Moreover, the depolarisation of the electrode is observed which leads to an improved energetic efficiency, i.e. lower energy consumption for the same gas yield or higher gas yield for the same level of energy consumption. It has to be kept in mind that during the water electrolysis there is an oxygen evolution reaction at the counter electrode which as shown by Matsushima et al. is affected by a superposed magnetic field the same way as hydrogen [12]. This means that these effects can be achieved at both electrodes leading to even greater energy efficiency and reduced production costs.

Acknowledgement

The German Research Foundation (DFG) is gratefully acknowledged for the support of this work in the framework of the

Collaborative Research Centre 609 “Electromagnetic Flow Control in Metallurgy, Crystal-Growth and Electrochemistry”.

References

[1] H. Cheng, K. Scott, C. Ramshaw, J. Electrochem. Soc. 149 (2002) D172.
[2] G.M. Whitney, C.W. Tobias, AIChE J. 34 (1988) 1981.
[3] M.G. Fouad, G.H. Sedahmed, Electrochim. Acta 18 (1973) 55.
[4] P. Mandin, J. Hamburger, S. Bessou, G. Picard, Electrochim. Acta 51 (2005) 1140.
[5] H. Vogt, Electrochim. Acta 38 (1993) 1421.
[6] H. Vogt, R.J. Balzer, Electrochim. Acta 50 (2005) 2073.
[7] C. Gabrielli, F. Huet, R.P. Nogueira, Electrochim. Acta 50 (2005) 3726.
[8] J. Eigeldinger, H. Vogt, Electrochim. Acta 45 (2000) 4449.
[9] C.W.M.P. Sillen, The effect of gas bubble evolution on the energy efficiency in water electrolysis. Dissertation, TU Eindhoven, 1983.
[10] R.J. Balzer, H. Vogt, J. Electrochem. Soc. 150 (2003) E11.
[11] T. Iida, H. Matsushima, Y. Fukunaka, J. Electrochem. Soc. 154 (2007) E112.
[12] H. Matsushima, T. Iida, Y. Fukunaka, Proc. 6th International Conference on Electromagnetic Processing of Materials, Dresden, Germany, 19–23 October, 2009, p. 502.
[13] H. Matsushima, D. Kiuchi, Y. Fukunaka, Electrochim. Acta 54 (2009) 5858.
[14] Z. Diao, P.A. Dunne, G. Zangari, J.M.D. Coey, Electrochem. Commun. 11 (2009) 740.
[15] R. Aogaki, K. Fueki, T. Mukaibo, Denki Kagaku oyobi Kogyo Butsuri Kagaku 43 (1975) 504.
[16] J.A. Koza, M. Uhlemann, A. Gebert, L. Schultz, Electrochem. Commun. 10 (2008) 1330.
[17] J.A. Koza, S. Mühlenhoff, M. Uhlemann, K. Eckert, A. Gebert, L. Schultz, Electrochem. Commun. 11 (2009) 425.
[18] K. Shinohara, K. Hashimoto, R. Aogaki, Electrochemistry 70 (2002) 773.
[19] PivView Software Manual, Göttingen, Germany.
[20] J.H. Ferziger, M. Peric, Computational Methods for Fluid Dynamics, 3rd ed., Springer, Berlin, 2002, p. 423.
[21] C.M. Rhie, W.L. Chow, AIAA J. 21 (1983) 1525.
[22] Ch.M.A. Brett, A.M.O. Brett, Electrochemistry. Principles, Methods, and Applications, Oxford University Press, Oxford/New York/Tokyo, 1994.
[23] H. Vogt, Electrochim. Acta 25 (1980) 527.
[24] O. Devos, A. Olivier, J.P. Chopart, O. Aaboubi, G. Maurin, J. Electrochem. Soc. 145 (1998) 401.
[25] S.V. Patankar, Numerical Heat Transfer and Fluid Flow, Hemisphere Publishing Corporation, 1980.
[26] C. Cierpka, T. Weier, G. Gerbeth, M. Uhlemann, K. Eckert, J. Solid State Electrochem. 11 (2007) 687.